Coarse-Grained Polymer Melts Based on Isolated Atomistic Chains: Simulation of Polystyrene of Different Tacticities

ARTICLE *in* MACROMOLECULES · OCTOBER 2009

Impact Factor: 5.8 · DOI: 10.1021/ma901242h · Source: OAI

Macromolecules
ARTICLE

Macromolecules **2009**, *42*, 7579–7588 **7579**
DOI: 10.1021/ma901242h

Coarse-Grained Polymer Melts Based on Isolated Atomistic Chains: Simulation of Polystyrene of Different Tacticities

Dominik Fritz, Vagelis A. Harmandaris, Kurt Kremer, and Nico F. A. van der Vegt*,†

Max-Planck-Institut für Polymerforschung, Ackermannweg 10, 55128 Mainz, Germany.
†Current address: Center of Smart Interfaces, Technische Universität Darmstadt, Petersenstrasse 32, 64287 Darmstadt, Germany.

Received June 10, 2009; Revised Manuscript Received September 2, 2009

ABSTRACT: We present a molecular coarse-graining approach applied to polystyrene which obtains both the bonded and nonbonded interactions of the coarse-grained model from the sampling of isolated atomistic chains and pairs of oligomers. Atomistic melt properties are not used in the parametrization. We show that the coarse-grained polystyrene model not only predicts melt properties, including the melt packing and the density between 400 and 520 K, in satisfactory agreement with the atomistic model, but also reproduces the local chain conformations of atactic as well as stereoregular polystyrene. The model takes into account and reproduces correlations between neighboring bonded degrees of freedom and therefore reproduces the conformations of detailed atomistic chains in the melt on all length scales.

1. Introduction

Coarse-grained (CG) polymer models for specific systems significantly extend the scope and applicability of molecular simulations in polymer science. Systematic coarse-graining approaches have received significant attention in recent years and usually obtain the parameters of the simplified CG model from simulations of a more detailed (all-atom or united-atom) model.[1−19] In combination with mapping procedures that link the different models, hierarchical simulations offer new opportunities to studying structure−property relations of chemically specific systems.

The development of CG particle models is an active field of research in different communities.[7] The common approach to obtain CG molecular models is to merge groups of chemically connected atoms into "superatoms" or CG beads (see Figure 1) and to derive effective CG interaction potentials by averaging over the atomistic degrees of freedom. The number of real atoms that are represented by one CG bead, the degree of coarse graining, can vary from a few atoms per bead up to models where many monomers are represented as a big blob[8,9] or a whole chain is modeled by an ellipsoid.[10] The choice of the appropriate model depends on the problem considered. If the degree of coarse graining is too high, the CG model may not be capable of describing properties linked to local details, for example, the conformation and packing of chain segments in the melt. Here we shall be concerned with CG models as the one shown in Figure 1. Although previously developed coarse-graining procedures yield CG models that are perfectly suited to equilibrate large length and time scales in molecular dynamics (MD) simulations, the models have limited predictive power (they cannot easily be transferred to conditions other than those for which they were developed). Limited transferability, apart from being inherent to any atomistic or CG model, is also owing to the coarse-graining method employed. More specifically, nonbonded bead−bead interactions of the CG model can be developed to reproduce target properties of a detailed-atomistic system (e.g., the bead−bead radial distribution function in the amorphous melt). With these potentials, however, it remains unclear if other properties can be reproduced which have not been used in the design of the potential. It also remains unclear if the coarse-graining procedures reported so far are sufficiently accurate to reproduce the chain conformations at each scale ranging between the local scale of a few repeat units and the global scale of the entire polymer. In this respect another unresolved issue is whether changes in conformation due to variations in stereoregularity can be realistically described on each of these scales with a single CG "mapping scheme". This question remains unresolved also in biomolecular simulations where only until very recently preliminary attempts have been made to derive CG potentials from atomistic models which are capable of predictively modeling local conformations (secondary structure) and changes thereof.[4,5] In this paper we describe a coarse-graining procedure for stereoregular polystyrenes yielding a CG model with greater predictability than the models reported so far.

Polystyrene (PS) is one of the most common commercial polymers. It is widely studied and an example of the large family of vinyl polymers. Different CG models for PS have previously been reported.[11−16] Several models use a 1:1 mapping scheme in which one CG bead represents one monomer.[11−14] Even though some of these models keep information about the chain stereosequences, they are only used to describe atactic polystyrene. All these models use iterative Boltzmann inversion (IBI)[17] to obtain the nonbonded interaction potentials. In the IBI method an initially guessed potential is iteratively refined until radial distribution functions (RDF) from CG simulations reproduce the target RDFs from atomistic melt simulations. In addition to the RDFs from atomistic simulations, the pressure can be used as a target quantity to be reproduced by the IBI potentials. Our previous polystyrene models[15,16] instead used repulsive (shifted) Lennard-Jones-type potentials which were tuned to fit RDFs obtained from atomistic melt simulations. These potentials turned out to be well-suited for the problems studied in these works and offered the computational advantage of (among others) being combined with short interaction cutoffs. Obviously, they cannot be used to study systems under ambient

*Corresponding author. E-mail: vandervegt@csi.tu-darmstadt.de.

Published on Web 09/11/2009

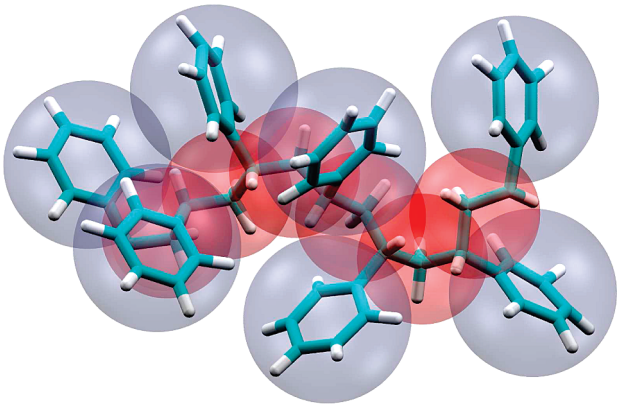

Figure 1. Mapping scheme: each monomer is mapped onto two coarse-grained beads. Bead A is the center of mass of the CH_2 group and the two CH groups, weighted with half of their masses. Bead B is the center of mass of the phenyl group. Figure created with VMD.[20]

pressure conditions or be applied to study interfacial phenomena and formation of ordered structures driven by enthalpic interactions.

In the following section we describe a coarse-graining procedure that is based on detailed all-atom simulations of stereoregular PS sequences in vacuum. One advantage of this approach is that it is computationally inexpensive. More importantly, however, we do not use information on properties of the melt state (that we wish to describe with the model) as input in the development of the effective potentials. The bonded as well as nonbonded CG potentials are obtained from independent simulations and as such are strictly separated. With this approach we aim at developing CG polymer models that exhibit greater transferability. In the results and discussion section we report conformational properties of atactic, syndiotactic, and isotactic PS at the level of several repeat units up to the level of the overall chain dimension. We also report properties of molten polystyrene as predicted by the CG model. The results are compared with the available experimental data.

2. Hierarchical Modeling

2.1. General Coarse-Graining Procedure. The assumption we start from is that the total potential energy, U^{CG}, for a CG chain can be separated in a bonded part, U^{CG}_{bonded}, and in a nonbonded part, $U^{CG}_{nonbonded}$

$$U^{CG} = \sum U^{CG}_{bonded} + \sum U^{CG}_{nonbonded} \quad (1)$$

After choosing a mapping scheme, we derive the bonded and nonbonded interaction potentials separately. For the bonded interactions the approach is based on sampling distribution functions from atomistic simulations of isolated random walks; for the nonbonded interactions the approach is based on sampling potentials of mean force between two short oligomers in vacuum. We do not use atomistic simulations of the condensed, melt state to develop our CG force field. Hence, our approach is principally different from CG methods that use condensed phase structures as a prerequisite input for the parametrization of the model. The typical methodology used here can be summarized in the following steps:

1. Atomistic MD or Monte Carlo (MC) simulations of isolated random walks are performed. At this point only local interactions are taken into account. For MD a Langevin thermostat is used to ensure proper equilibration.

2. After sampling a large number of independent conformations for the PS random walks at a given temperature T, probability distribution functions $P^{CG}(r,\theta,\phi,T)$ are obtained, which are, in general, unknown functions of the CG bond length r, bending angles θ, and dihedral angles ϕ. The standard way to proceed in order to calculate the CG force field parameters is to assume that $P^{CG}(r,\theta,\phi,T)$ factorizes as

$$P^{CG}(r,\theta,\phi,T) = P^{CG}(r,T)P^{CG}(\theta,T)P^{CG}(\phi,T) \quad (2)$$

This assumption is only valid if the internal CG degrees of freedom are uncorrelated. In this respect, the choice of the CG mapping scheme is crucial. We will discuss in the following that we find correlations in our model, but by carefully choosing beyond which distance to cut off local interactions along the backbone in the atomistic sampling (step 1) and choosing a suitable set of bonded interactions, our CG model is able to preserve the correlations that the atomistic model shows. This enables us to proceed with this methodology.

3. Having the probability distribution functions, the CG bonded potentials are given from the inverse Boltzmann relations

$$U^{CG}(r,T) = -k_B T \ln P^{CG}(r,T) \quad (3)$$

$$U^{CG}(\theta,T) = -k_B T \ln P^{CG}(\theta,T) \quad (4)$$

$$U^{CG}(\phi,T) = -k_B T \ln P^{CG}(\phi,T) \quad (5)$$

In the above expressions the probability distribution functions for bond length and bending angle are normalized by taking into account the corresponding volume elements r^2 and $\sin\theta$.

4. Finally, the CG force field is completed by adding a nonbonded interaction potential. We previously used Lennard-Jones-type potentials with heuristically modified exponents.[16] In this work we develop effective nonbonded potentials in a tabulated form, based on calculations of potentials of mean force between two short oligomers.

2.2. Mapping Scheme. The mapping scheme was already used for the previous model for polystyrene.[16] It maps each monomer onto two coarse-grained, spherical beads of different types (see Figure 1):

- **Bead A** contains carbon atoms in the backbone connecting two subsequent phenyl rings and hydrogen atoms attached to these carbon atoms. The CH groups in the backbone to which the phenyl rings are attached, belong to two neighboring A beads. The center of bead A is the center of mass of the CH_2 group and the two CH groups, which are taken with half of their masses.
- **Bead B** contains the atoms of the phenyl group. The center of bead B is mapped onto the center of mass. The beads are connected by CG bonds A−B between the alternating types of beads. This leads to a chain without side groups. There are no bonds A−A or B−B between neighboring beads of the same type.

In the development of the CG model we distinguish between the different tacticities of polystyrene. Pairs of two subsequent monomers in PS can have two different orientations (see Figure 2). In a meso diad both phenyl rings are pointing to the same side (assuming all-trans configuration of the backbone). A chain consisting only of meso diads is isotactic. In racemic diads the phenyl rings point to opposite sides. A chain consisting only of racemic diads is syndiotac-

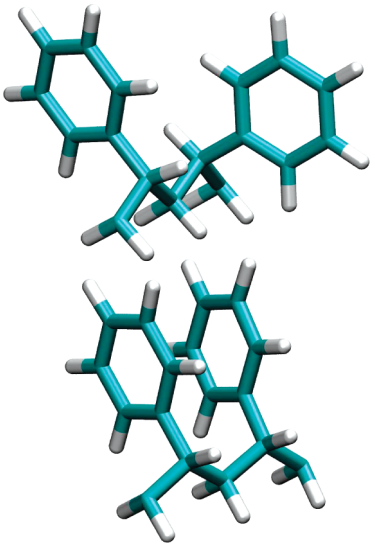

Figure 2. Diads in polystyrene: in racemic diads (upper) the phenyl rings point to different sides, and in meso diads (lower) they point to the same side (assuming an all-trans configuration of the backbone).

tic, having the phenyl rings along the chain pointing to alternating sides. In atactic chains the types of diads are randomly distributed.

The choice of a mapping scheme is not unique, and in the case of the 1:1 mapping scheme different choices were taken: Milano and Müller-Plathe[11,12] center the superatoms on methylene carbons and distinguish between two types of beads according to the diad they belong to. This model is able to keep information about the chain stereosequences while reducing the description of local conformations to angular potentials. The model of Qian and co-workers[13] places the superatoms on the center of mass of the monomers. Two different bead types represent the orientations of the side groups and keep information about the chain stereosequences. It is also used to study mixtures of PS and ethylbenzene.[13] Sun and Faller[14] center the superatoms on the backbone carbons to which the phenyl rings are attached and use a single type of bead to describe atactic polystyrene.

2.3. Bonded Potentials. Potentials for bonded degrees of freedom of the CG model are obtained by direct Boltzman inversion (see eqs 3−5) of distributions obtained from all-atom simulations of single chains in vacuum using stochastic dynamics. All single chain sampling runs were performed with 25-mers at a temperature of 503 K using the all-atom force field of Müller-Plathe.[21] The bonded potentials are developed for isotactic and syndiotactic polystyrene separately. Our aim is to still use the ansatz of factorizing the distribution functions.

Since the distribution functions of the bonded degrees of freedom are determined by interactions along the chain at a short-range only, we exclude long-range interactions and effectively sample random walks. The range of the atomistic potential used in this sampling procedure critically determines our ability to reproduce "local conformations" at the level of a few neighboring repeat units and is further discussed below.

2.3.1. Interaction Range along the Chain. In the previous CG model[16] bonded interactions up to 1−4 torsions were taken into account. All longer ranged CG interactions starting from 1 to 5 upward were modeled by repulsive nonbonded interactions, which were chosen the same as those used to describe interchain nonbonded interactions between CG beads in the melt. To develop the bonded potentials of the CG model, an all-atom model of the chain was sampled in vacuum with an atomistic force field that excludes all atom−atom nonbonded pair interactions along the chain falling outside the "1−4 range" of the CG chain description. We investigated the influence of the "interaction range" applied in the sampling of the single chains closer.

The influence of the interactions that we include in the sampling on the local distributions is shown in Figure 3 for the example of the BAB angle in fully isotactic and syndiotactic chains. We see that in both cases the form of the distribution changes for interaction ranges up to 1−5 and stays the same if we add atomistic interactions corresponding to the 1−6 CG level or beyond. By including the interaction range 1−5 we take into account the pentane effect between the backbone atoms in the A beads, and we avoid an overlap of the phenyl groups of the B beads in the 1−5 range.

We tested whether a CG model of an isolated chain with bonded potentials sampled with an "1−4 interaction range" and CG nonbonded interactions for the 1−5 neighbors could reproduce the distributions from a sampling with an "1−5 interaction range". We found that the distributions do not agree but stay the same as in the atomistic sampling with the "1−4 interaction range".

2.3.2. Correlations in Single Chains. The reason why the distributions of CG angles and dihedral angles do not change their general form when the "interaction range" is extended beyond 1−5 becomes clear if we look at dihedral−dihedral correlation plots in Figure 4. These plots show the probability distribution of two subsequent CG dihedral angles, which we find by sampling a single atomistic chain in vacuum and analyzing it in the CG description.

The longer we choose the range of interactions to include, the more combinations of dihedral angles are suppressed in the sampling of the local distributions. But as soon as the 1−5 interactions are included, we sample always the same combinations even if we include additional longer ranged interactions. This means that the interactions up to 1−5 determine correlations of the single chains as well as local conformations, as described before. Interactions between 1−6 neighbors and above might slightly influence the peak heights but not the peak positions. Beyond 1−5, the additional interactions only contribute to excluded volume effects. Since we describe the excluded volume interaction separately with nonbonded potentials (section 2.4), it seems reasonable to include interactions at least up to 1−5 in our sampling of the single chains from which the CG bonded potentials are obtained. We performed the atomistic sampling of single chains with all interactions included up the 1−6 CG level in the derivation of the CG bond, angle, and torsion potentials. By that we extend the path, that was followed before,[15,16] to include only interactions up to 1−4 in the atomistic single-chain sampling. Graphs of the bonded potentials can be found in the Supporting Information.

2.3.3. Bonded Interactions beyond 1−4. After extending the range of interactions in the sampling of the atomistic chains, we describe in the following our method to obtain bonded potentials in a range beyond 1−4. The introduction of CG bonded potentials beyond 1−4 improves the model to reproduce local conformations, in case these potentials are different from the CG nonbonded pair potentials, which would be used otherwise. This difference can be expected, since neighboring beads belonging to the same chain will have a different average orientation toward each other than two close beads belonging to different chains, which is the case for which the CG nonbonded potentials are developed. The second aim of the longer ranged bonded potentials is to induce a stiffness of the chain, which compares to the

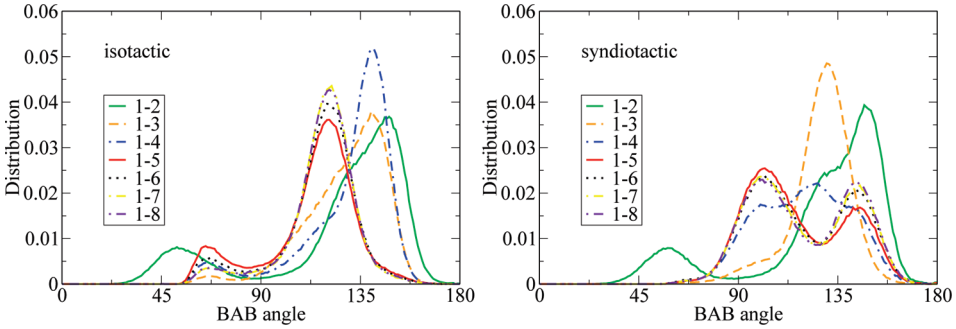

Figure 3. Distributions of BAB angles in fully isotactic (left) and fully syndiotactic (right) single chains in vacuum; the interaction range in these all-atom runs was varied to correspond with CG interactions in a range from 1−2 to 1−8; for 1−5 and above the peak positions stay the same. All distributions in this figure as well as all following distributions for CG degrees of freedom in this work are normalized.

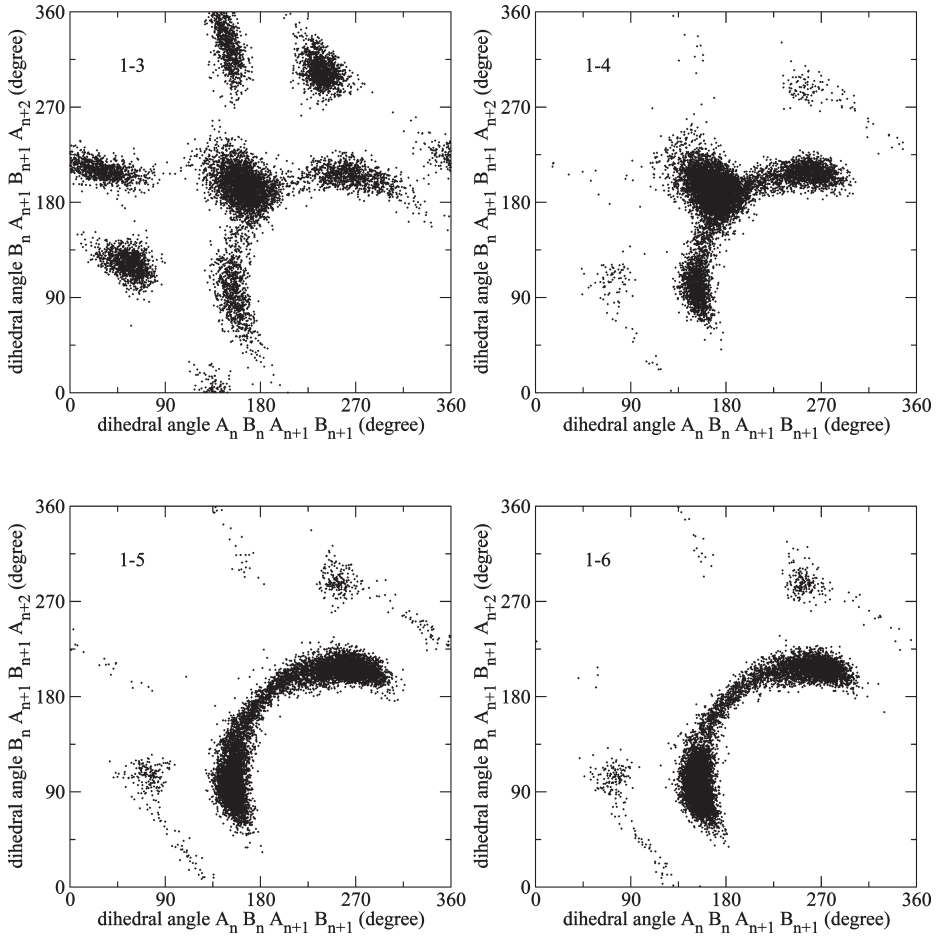

Figure 4. Combinations of two subsequent CG dihedral angles in a single, isotactic chain. The two dihedrals share three beads, which form an angle BAB, and include as fourth bead the A beads next to this BAB angle. Shown are the combinations of dihedral angles with varied range of interactions along the chain. 1−3 interactions (upper panel, left), 1−4 interactions (upper panel, right), 1−5 interactions (lower panel, left), 1−6 interactions (lower panel, right). By including the interactions 1−4 and 1−5 several combinations are suppressed. For better visibility the dihedral values in the range from −180° to 0° are shifted to the range from 180° to 360°.

stiffness of the atomistic chain. These potentials are developed starting with 1−5 potentials and can be extended stepwise to 1−6 or even 1−7 interactions.

These bonded potentials potentials are distance dependent pair potentials, contrary to angular and torsional potentials, which act on groups of three or four CG beads. The difference between the 1−5 interactions and the shorter bonded interactions is that by construction they are not completely decoupled, which was one of the basic assumptions before. Given a certain set of values for intermediate bonds, angles, and dihedral angles, the distance between two 1−5 neighbors in the chain is completely determined. On the other hand, a certain 1−5 distance can be realized with several combinations of intermediate bonds, angles, and dihedrals. The fact that 1−5 distances and shorter bonded interactions are not decoupled can be seen as well, if we look at a single CG chain in vacuum, which has only bonded potentials for CG bonds, angles, and dihedral angles and no bonded or nonbonded interactions with a longer range. If for one degree of freedom, say, an angle, we switch off the potential, the sampling of the CG chain will show a uniform distribution for this degree of freedom (after normalizing

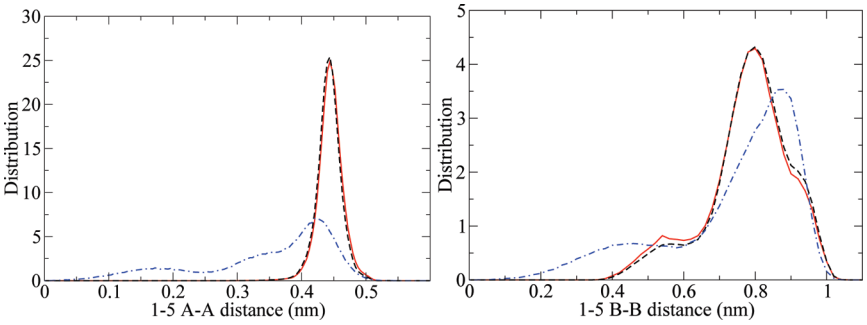

Figure 5. Distributions of 1−5 distances in isotactic chains for A−A (left) and B−B (right) beads: the target distribution from an all-atom single chain (dashed), the correcting distribution from a CG chain with bonded interactions up to 1−4 (dashed-dotted), and final CG distribution of a CG chain with the additional corrected 1−5 potentials (continuous).

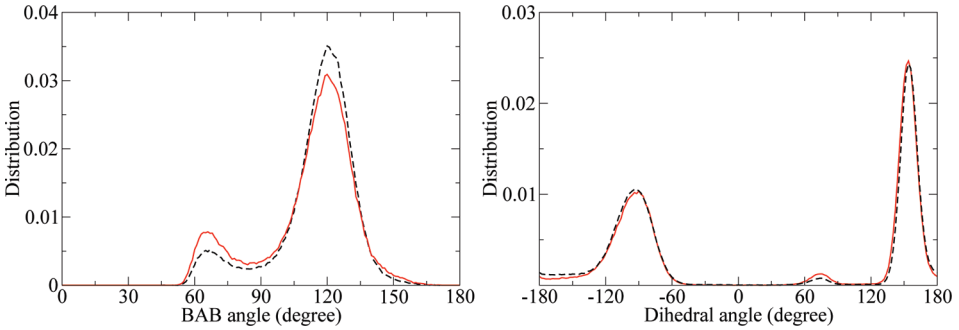

Figure 6. Distributions for angles (left) and dihedral angles (right) in isotactic chains in comparison for all-atom single chains (dashed) and CG chains (continuous) with bonded 1−5 interactions. This comparison shows that angles and dihedral angles are not deviating significantly when we introduce bonded 1−5 interactions in the CG model.

with sin θ). The sampled distribution of 1−5 distances, however, will not be uniform, although there is no direct interaction present between the two beads. This influence of the intermediate interactions up to 1−4 has to be taken into account, when we develop the 1−5 CG potentials. In Figure 5 these distributions are shown for A−A and B−B 1−5 distances in a isotactic CG chain, having only bonded interactions up to 1−4 (dashed-dotted line), denoted by $P^{1-5,\mathrm{A-A}}_{\mathrm{correcting}}(r,T)$ for the A−A case. If we only Boltzmann-invert the 1−5 distributions (dashed lines) from the sampling of an atomistic chain including the 1−5 range, denoted by $P^{1-5,\mathrm{A-A}}_{\mathrm{target}}(r,T)$, we would double count the contribution of the CG bonded interactions up to 1−4 (dashed-dotted line). Therefore, we Boltzmann-invert the 1−5 distance distribution from a single all-atom chain, which is our target distribution, and subtract the Boltzmann-inverted 1−5 distribution of a CG chain having only bonded interactions up to 1−4:

$$U^{\mathrm{CG}}(r,T) = -k_{\mathrm{B}}T[\ln P^{1-5,\mathrm{A-A}}_{\mathrm{target}}(r,T) - \ln P^{1-5,\mathrm{A-A}}_{\mathrm{correcting}}(r,T)] \quad (6)$$

With these corrected potentials we can sample 1−5 distributions in CG chains, which are in very good agreement with the distributions of the all-atom chain (continuous line in Figure 5). The effect of the 1−5 bonded interactions on the intermediate bonded distributions of angles and dihedral angles is shown in Figure 6. We can see that the distributions do not deviate strongly.

Since we have to types of 1−5 interactions, A−A and B−B, they also may influence each other. For the isotactic case presented here, this is a minor effect. For the syndiotactic case the correcting potential $P^{1-5,\mathrm{B-B}}_{\mathrm{correcting}}(r,T)$ has to be sampled from a CG chain including bonded potentials up to 1−4 and the 1−5 A−A potential and vice versa. This process of correcting the potentials can be done iteratively. For the syndiotactic case it was sufficient to do three steps. Details and the distributions for syndiotactic chains can be found in the Supporting Information.

Extending this scheme to 1−6 interactions or above is straightforward. The Boltzmann-inverted distribution for the 1−6 distance from a single all-atom chain is corrected by the Boltzmann-inverted distribution of a CG chain, which includes only interactions up to 1−5, and so on. For fully isotactic and syndiotactic chains we used bonded interactions up to 1−7, which is necessary to impose the right stiffness of the chains. For atactic chains it is sufficient to use bonded 1−5 potentials.

Figure 7 shows the probability distributions of two subsequent dihedral angles in an isolated, isotactic 25-mer simulated with the all-atom model and with the corresponding CG model. The all-atom chain includes all interactions along the chain; the CG chains includes CG bonded potentials up to 1−5 and CG nonbonded potentials (section 2.4) for 1−6 interactions and beyond. The agreement is very good; all regions sampled by the atomistic chain are reproduced by the CG chain, except for the region around (160°, 200°). More important, however, the CG chain does not sample the region (270°, 90°), indicating that our final CG model reproduces the local correlations between adjacent torsional degrees of freedom in polystyrene.

2.3.4. Extension and Transfer: 1−5 Potentials in Atactic Chains. In the next step we checked how the different sets of bonded potentials for purely iso- and syndiotactic chains can be combined to simulate chains which include meso diads and racemic diads. In atactic chains these diads are randomly distributed. We therefore checked whether the local distributions for bonds, angles, and dihedrals only depend on the type of diad which is involved in these sequences of 2, 3,

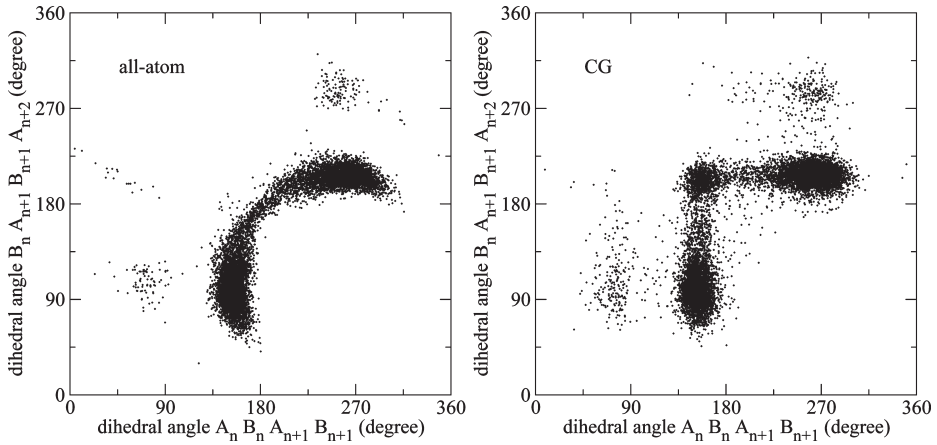

Figure 7. In comparison to Figure 4: combinations of dihedral angles for an isotactic single chain including all intrachain interactions of the all-atom model (left) and for a CG chain with bonded potentials up to 1−5 (taken from a sampling including the 1−5 range) and nonbonded CG potentials beyond (right).

or 4 CG beads or if the neighboring diads have a strong influence, too.

We investigated a chain consisting of a sequence of diads of alternating meso and racemic type. In this chain, the phenyl rings are pointing pairwise to alternating sides. Each diad has two neighboring diads of the opposite type. It turned out that the neighboring diads do not influence local distributions of CG bonded degrees of freedom significantly. These distributions and details are shown in the Supporting Information.

Since the local distributions mainly depend on the local tacticity and not on the tacticity of the neighboring diads, we can describe atactic chains by combining the previously described potentials for isotactic and syndiotactic chains.

2.4. Nonbonded Potentials. As discussed in the Introduction, one of the goals of the present work is to develop a CG model that can be used under ambient pressure conditions. For this reason we develop nonbonded interactions including an attractive tail as opposed to the purely repulsive potentials that were used for the previous model.[16] These effective potentials are obtained from constraint dynamics runs with the all-atom model of two trimers (or fourmers) in vacuum, between which we calculated the pair potential of mean force (PMF) along a distance coordinate r connecting the CG mapping points of selected central A or B beads. The PMF, V_{PMF}, between the two oligomers was calculated from n distance constraint simulations, using the following equation:

$$V_{\mathrm{PMF}}(r) = \int_{r_m}^{r} [\langle f_c \rangle_s] \, \mathrm{d}s + 2k_B T \ln r \qquad (7)$$

where k_B is the Boltzmann constant, T is the temperature, f_c is the constraint force between the two selected central bead CG mapping points, and r_m is the maximum distance between the two mapping points (r varies from 0.2 to 1.2 nm in steps of 0.02 nm). Because only the distance between the two mapping points is constrained, free rotation of the oligomer−oligomer connecting vector remains possible and larger volume elements are sampled at larger distances. This leads to an entropy contribution to the averaged constraint force that must be subtracted out. The second term on the right-hand side of eq 7 takes care of this contribution.

The obtained PMF is denoted $V_{\mathrm{PMF}}^{\mathrm{AA}}(r)$ (for the case we constrain the A−A distance). To obtain an effective A−A interaction potential $V_{\mathrm{eff}}^{\mathrm{AA}}(r)$, we calculate a second PMF

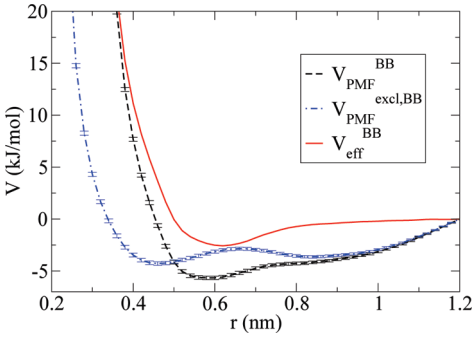

Figure 8. Coarse-grained B−B nonbonded interaction: the two potentials of mean force for runs with all interactions (dashed) and for reruns with exclusions between all atoms of the B beads (dashed-dotted) as well as the effective potential, obtained by taking the difference of the two potentials of mean force (continuous).

along the same coordinate r but exclude all direct A−A atomistic interactions while maintaining all other interactions with and between neighboring parts of the oligomers. This PMF we denote $V_{\mathrm{PMF}}^{\mathrm{excl,AA}}$. The effective, nonbonded bead−bead interaction potential is next obtained from

$$V_{\mathrm{eff}}^{\mathrm{AA}}(r) = V_{\mathrm{PMF}}^{\mathrm{AA}}(r) - V_{\mathrm{PMF}}^{\mathrm{excl,AA}}(r) \qquad (8)$$

The so-obtained potential $V_{\mathrm{eff}}^{\mathrm{AA}}(r)$ may be viewed as the free energy of introducing intermolecular interactions between the two groups of atoms representing the A beads at distance r. Because bead A is part of an oligomer (trimer, fourmer), steric effects due to chain connectivity limit the set of relative orientations in which these beads can approach, which is realistically captured by V_{eff}. Although V_{eff} is a pair potential obtained from PMF calculations between PS fragments in vacuum, its use in simulations of the condensed melt state can be justified. Multibody contributions to the effective potential applicable in the melt are to a large extent similar to those present in vacuum and are determined by the relative orientations chain segments can sample relative to one another. As a final technical note we point out that $V_{\mathrm{PMF}}^{\mathrm{excl,AA}}(r)$ was obtained by using the simulation trajectories of the first run (used to determine $V_{\mathrm{PMF}}^{\mathrm{AA}}$) and recalculating the forces for the given conformations but excluding the direct interactions between the two beads at fixed distances.[22] Figure 8 shows the two potentials of mean force, $V_{\mathrm{PMF}}^{\mathrm{BB}}$ and $V_{\mathrm{PMF}}^{\mathrm{excl,BB}}$, and the resulting effective potential $V_{\mathrm{eff}}^{\mathrm{BB}}$

for the interaction between the phenyl beads. In principle, the above procedure can be iterated to reproduce the all-atom AA, AB, and BB PMFs of trimers (or fourmers) in vacuum with the effective AA, AB, and BB potentials. Such an approach has been used before by McCoy and Curro[23] to derive united-atom models for small molecules and resembles the IBI approach which is often used in the melt.[17] Similar approaches have been used in the past to develop CG nonbonded interactions for polyethylene[24] and lattice systems.[25]

We note that the effective potential may change if, instead of the distance between the exact mapping points, the distance between the centers of mass of the two beads (neglecting that the CH groups are only weighted with half of their mass) is used as distance coordinate. For our model, this is of course only an issue if the center of mass of the A bead is used, calculated with the full masses of the two CH groups instead of their half masses. Test calculations showed that this difference is indeed significant, leading to very different effective A−A and A−B nonbonded interaction potentials. Another important question is, which all-atom interactions need to be excluded in the calculation of $V_{\mathrm{eff}}^{\mathrm{excl,AA}}$ and $V_{\mathrm{eff}}^{\mathrm{excl,AB}}$? Because each of the two CH groups in a A-type bead is shared with another A bead, we have two choices. We can exclude the all-atom interactions involving only the CH_2 group or exclude the all-atom interactions involving the CH_2 and the CH groups. If we consider the A−A CG interaction, the first choice leads to an effective potential in which the contributions of the CH groups are not accounted for and the second choice leads to an effective A−A potential in which the contributions of the CH groups are counted twice. We calculated the effective potentials with both choices for treating the CH groups and took their linear average as the effective potential in further simulations. In our simulations of CG PS melts we get the best agreement with detailed atomistic structures of the melt (A−A, A−B, and B−B radial distribution functions) if we take the linear average of the two effective potentials.

The potentials obtained by this method combine a short-range repulsive and longer-ranged attractive part and are used for the melt simulations discussed below. The B−B nonbonded potential was obtained from PMF calculations of two trimers in which the coordinate r was chosen between the central B beads. The A−A nonbonded potential was calculated from PMF calculations of two fourmers in which the coordinate r was chosen between the central A beads. To determine the A−A nonbonded interaction potential, trimers are too small and exhibit a nonsymmetric environment around the central A bead. The A−B nonbonded potential was obtained based on PMF calculations with a fourmer (A bead) and a trimer (B bead). In all calculations the stereoregular sequence was isotactic. The potentials were also calculated with syndiotactic sequences, which yielded nonbonded potentials that were identical within the error bars. In Figure 9 the effective potentials are plotted for the three interaction pairs A−A, A−B, and B−B for isotactic oligomers. The short-range repulsion for the B−B interaction is "softer" than for the A−A interaction because the level of coarse graining of the B bead (11 atoms) is larger than that of the A bead (5 atoms).

3. Atomistic and Coarse-Grained Simulations

3.1. Atomistic MD Simulations. All simulations reported in this study were performed using the molecular dynamics package GROMACS.[26] For the atomistic modeling of polystyrene the all-atom model of Müller-Plathe was used.[21]

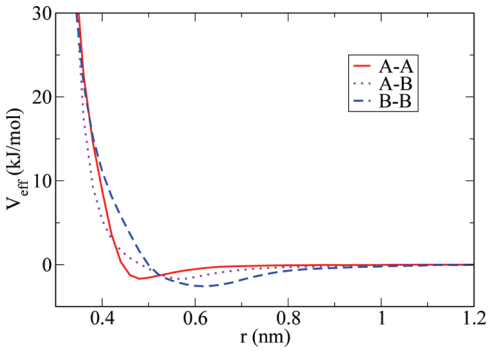

Figure 9. Nonbonded potentials: comparison of tabulated potentials used in this work: A−A (continuous), A−B (dotted), B−B (dashed).

Table 1. All-Atomistic PS Systems Studied in This Work[a]

N_{monomers}	N_{chains}	tacticity	T (K)	C_N	ρ (kg/m^3)
10	56	atactic	503	6.09	959
10	56	isotactic	503	6.12	956
10	56	syndiotactic	503	7.70	959
10	56	atactic	403		1004
10	56	atactic	423		1000
10	56	atactic	443		989
10	56	atactic	463		980
10	56	atactic	483		969
10	56	atactic	503		960
10	56	atactic	523		947

[a] Reported are the number of repeat units per chain N_{monomers}, the number of chains in the simulation box N_{chains}, the tacticity of the chains, and the temperature T as well as the resulting characteristic ratio between the two end beads of the chain C_N (where $N = 2N_{\mathrm{monomers}} - 1$) and the density ρ.

Every PS monomer is described by 16 atoms. For nonbonded interactions a cutoff distance of 1 nm was used. Cutoff corrections were applied to energy and pressure using standard analytical expressions that assume a uniform density beyond the cutoff.[27] Coulombic interactions beyond the cutoff were treated by reaction-field correction with a dielectric constant $\varepsilon_{\mathrm{RF}}$ of 2.5. All bond lengths were constrained using the LINCS method.[28] All atomistic MD melts were simulated under isothermal−isobaric (NpT) conditions at 503 K and 1 atm using the Berendsen thermostat (coupling time 0.2 ps) and barostat (coupling time 2.0 ps).[29] The integration time step was 1 fs. We simulated PS melts of isotactic, syndiotactic, and atactic tacticity. Each system consisted of 56 chains of 10 monomers. All systems are listed in Table 1. The initial configurations for the iso- and syndiotactic systems have been obtained by randomly placing 56 single chains in a box and slowly switching on the nonbonded interactions. For the atactic system we used an existing configuration of Milano and Müller-Plathe. After the first equilibration of the systems production runs of 400 ns were performed.

3.2. Coarse-Grained MD Simulations. For the coarse-grained simulations in this work bonded and nonbonded potentials were used in a tabulated form, which is implemented in GROMACS 4.[26] For nonbonded interactions a cutoff distance of 1 nm was used. CG melts were simulated under isothermal−isobaric (NpT) conditions at 503 K and 1 atm using the Berendsen thermostat (coupling time 0.4 ps) and barostat (coupling time 4.0 ps).[29] Here we use the same pressure as in the atomistic case. This is not necessarily the best way to go on since especially for nonbonded interactions it is difficult to adjust compressibility and pressure at the same time.[30] Systems of long chains (192 monomers) were simulated under NpT conditions for 80 ns and then

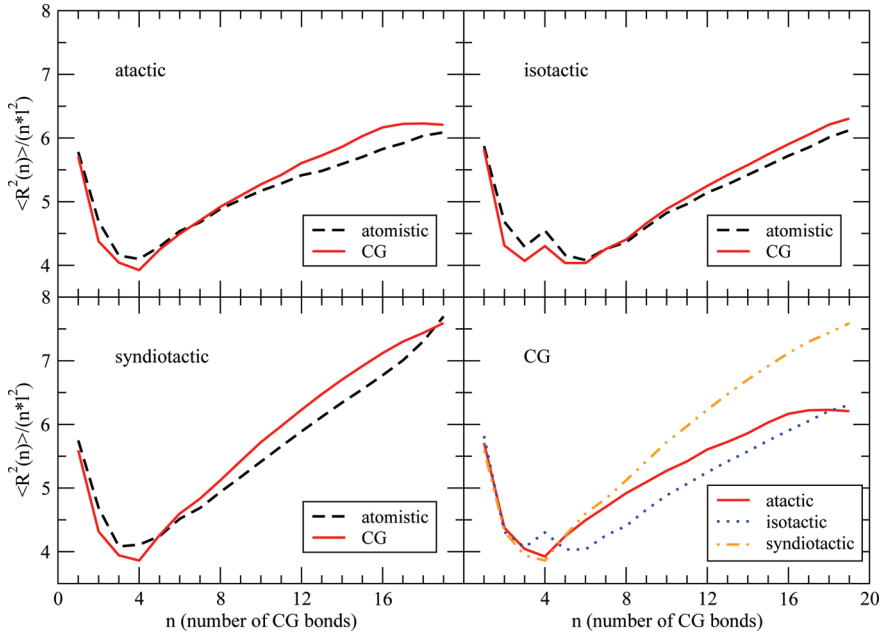

Figure 10. Simulations of 10-mer melts: internal distances for atactic (upper left), isotactic (upper right), and syndiotactic (lower left) PS melts comparing CG (continuous line) and all-atom simulations (dashed) and comparison between the CG systems with different tacticities (lower right). Plotted are the averages of the squared distances between beads, separated by n bonds, divided by the number of CG bonds and the squared bond length l^2. Since the number of CG bonds is equal to the number of carbon−carbon bonds in the backbone of the atomistic model, we normalize the CG distances also with the atomistic carbon−carbon bond length l of 0.153 nm.

simulated under NVT conditions at the average density of the first 80 ns. The integration time step was 3 fs. Here we have to note that the dynamics and therefore also the time scale of the CG system are systematically different and much faster than the dynamics in atomistic simulations.[16] We simulated CG melts of chains of 10 and 192 monomers with isotactic, syndiotactic, and atactic tacticity. All CG systems modeled in this study are presented in Table 2. As an initial configuration for the melts of long chains we used an atactic system, which was equilibrated with our previous model using the setup as described there.[16,31] The setup of the CG melts of shorter chains is not critical because the chains move their own size during a first equilibration run of a few nanoseconds.

Table 2. Coarse-Grained PS Systems Studied in This Work[a]

$N_{monomers}$	N_{chains}	tacticity	T (K)	C_N	ρ (kg/m^3)
192	50	atactic	503	7.80 ± 0.38	1035
192	50	isotactic	503	8.91 ± 0.30	1040
192	50	syndiotactic	503	12.27 ± 0.30	1031
10	56	atactic	503	6.21	964
10	56	isotactic	503	6.30	968
10	56	syndiotactic	503	7.59	962
10	56	atactic	403	6.97	1010
10	56	atactic	423	6.73	1001
10	56	atactic	443	6.55	992
10	56	atactic	463	6.48	983
10	56	atactic	483	6.25	973
10	56	atactic	503	6.23	964
10	56	atactic	523	6.06	954

[a] Reported are the number of repeat units per chain $N_{monomers}$, the number of chains in the simulation box N_{chains}, the tacticity of the chains, and the temperature T as well as the resulting characteristic ratio between the two end beads of the chain C_N (where $N = 2N_{monomers} - 1$) and the density ρ.

4. Melt Simulations

4.1. Conformations in Melts. To compare the chain conformations in CG and atomistic melts, we look at the internal distances within the chains. They are described by the characteristic ratio $C_n = \langle R^2(n)\rangle/(nl^2)$, where $\langle R^2(n)\rangle$ is the mean-square distance between two monomers separated by n carbon−carbon bonds (two per monomer) of length l along the backbone. For the CG systems we use the atomistic bond length l = 0.153 nm and have as well two CG bonds per monomer; therefore, we can compare the internal distances for atomistic and CG systems directly and with experimental values for C_∞. For atomistic systems we apply the mapping scheme and evaluate the internal distances between the mapping points.

In Figure 10 the internal distances in atactic, isotactic, and syndiotactic melts of 10-mers are shown. Each melt consists of 56 chains with a length of 10 monomers simulated at 503 K. We used the bonded potentials which were described before. The atactic melt includes bonded 1−5 interactions; the stereoregular melts include bonded interactions up to 1−7 (1−7 A−A for isotactic and 1−7 A−A and B−B for syndiotactic systems). For intrachain interactions 1−6 and higher, as well as for interchain interactions, the effective nonbonded potentials were employed. We see that our CG model reproduces the internal distances for the melts of different tacticities. The agreement already in the short internal distances indicates that the local conformations in the CG systems are correct. The increase of the distances along the chain, especially the differences for different tacticities, suggests that the stiffness of the atactic, isotactic, and syndiotactic chains is modeled properly. This is important for melts of longer chains, where the characteristic ratio reaches a limit of C_∞, which can be compared to experimental results.

Figure 11 shows internal distances of CG melts of chains of 192 monomers. The influence of the different tacticities can be seen clearly. The internal distances reach a plateau for about half the number of monomers in the chain already. Therefore, we can compare the internal distances there with experimental results for the characteristic ratio C_∞. We get 7.8 for the C_∞ of atactic PS, 8.9 for isotactic PS, and 12.3 for syndiotactic PS. Experimental values are around

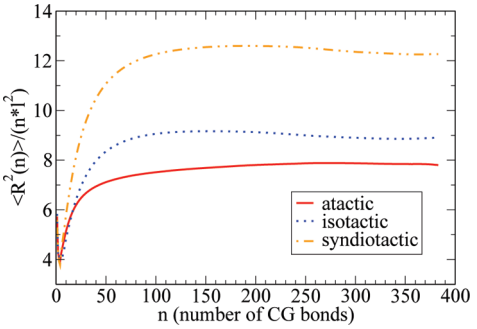

Figure 11. Melt simulations: internal distances for CG melts of chains of 192 monomers with different tacticities: atactic (continuous line), isotactic (dotted), and syndiotactic (dash-dotted).

9.1 ± 0.4 for atactic PS,[32] 9.3 for isotactic PS,[33] and 14.4 ± 2.8 for syndiotactic PS.[34,35] The simulated C_∞ for syndiotactic PS is higher than the value of 9 reported by Milano and Müller-Plathe in ref 11. Their model is developed from stereoregular sequences in an atactic polymer, which might explain the difference in the syndiotactic case, whereas their atactic value of 8 is in agreement with our model. The relative differences between the characteristic ratios of the different tacticities agree also with the rotational isomeric state (RIS) model, which predicts values of 9 for atactic PS, 12 for isotactic PS, and 18 for syndiotactic PS.[36] Even though our simulations, as well as experiments, show lower values for C_∞ than the RIS model for the stereoregular cases, we also observe that the atactic C_∞ is lower than the stereoregular cases, and we find almost the same ratio between the C_∞ for isotactic and syndiotactic PS.

4.2. Packing and Density in Melts. Next we examine local packing by calculating radial distribution functions (RDF). In Figure 12 RDFs between A−A, A−B, and B−B pairs for an atactic 10-mer melt are shown. In these RDFs only intermolecular pairs were included; pairs of beads in the same chain are left out, since the intrachain distributions are already reflected by the internal distances in Figure 10. We see very good agreement between all-atomistic and CG RDFs for distances below 0.5 nm. For larger distances the agreement is still good with some deviations. The strongest deviation appears for the B−B RDF, where the position and height of the first peak and the following minimum differ from the atomistic RDF. The reason for this might be the representation of the atomistic phenyl group by a spherical CG bead. This has been also observed with our previous CG PS model.[16] The RDFs for isotactic and syndiotactic melts show a very good agreement as well and can be found in the Supporting Information. We note that the CG simulations reproduce the small differences in the RDFs that atomistic simulations exhibit for different tacticities.

The density of the atomistic melt of atactic 10-mers (959 kg/m^{-3} at 503 K) is significantly above the reported experimental density of 895 kg/m^{-3} for short polystyrene chains (M_w = 910, M_w/M_n = 1.16).[37] Taking into account the M_w distribution and the slightly shorter chain length (around 9-mers), the atomistic melt density is around 5% to high. To be more close to experimental results one may have to adjust the density. Especially the dynamics of atomistic systems react sensitively to density changes.[19]

To test the temperature transferability of the CG model, we performed a series of runs over a range of temperatures from 403 up to 523 K. The densities predicted by the atomistic and CG models are shown in Figure 13. The CG model shows the same thermal expansion coefficient as the atomistic model, while the density is slightly overestimated

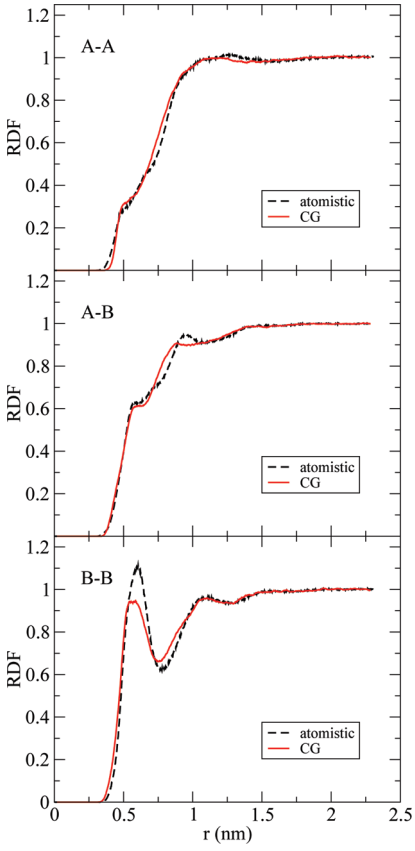

Figure 12. Radial distribution functions in atactic melt in comparison between CG (continuous lines) and all-atom simulation (dashed lines).

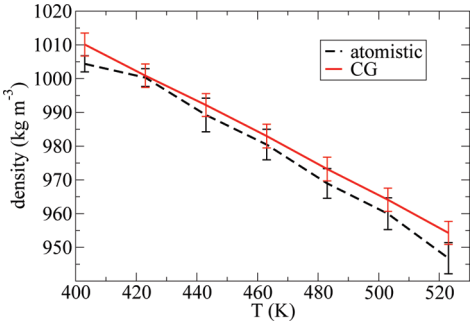

Figure 13. Densities obtained from constant pressure (1 atm) atomistic (dashed line) and CG simulations (continuous line) of a melt of 10-mers in a temperature range from 403 to 523 K.

compared to the prediction of the atomistic model. The agreement is strikingly good. A recent investigation by Qian and co-workers on the temperature transferability of another coarse-grained polystyrene model developed based on the iterative Boltzmann inversion method showed a similar good agreement between the thermal expansion coefficients of atomistic and coarse-grained melts.[13] There, the authors show that with another location of the CG mapping point (on the methylene unit rather than the bead center of mass) the temperature transferability is significantly worse.[38]

Coarse-grained models usually have state-dependent potentials because left-out degrees of freedom are weighted differently at different temperatures. The agreement we observe between the atomistic and coarse-grained model predictions over the wide range of temperatures shown in Figure 13 is achieved with a CG model developed at 503 K. This indicates that the temperature dependence of the CG

potentials must be quite weak, which we confirmed by reparameterizing the model at 423 K.

5. Conclusion

We presented a coarse-graining methodology which has been applied to the exemplary case of polystyrene and has the following features:

- It bases on a new approach to introduce longer-ranged intrachain potentials and to develop nonbonded potentials.
- It models atactic as well as stereoregular (isotactic and syndiotactic) polystyrene.
- Local chain conformations, chain stiffness, and overall chain dimensions are described in agreement with the detailed atomistic model. Overall chain dimensions, as the characteristic ratio C_∞, agree as well with experimental results for atactic and stereoregular polystyrene.
- The CG model describes the melt packing and reproduces the density at ambient pressure between 400 and 520 K, in good agreement with the atomistic model.
- The development of the model is computationally inexpensive because it is based on the sampling of isolated atomistic chains or pairs of oligomers in vacuum. No expensive atomistic melt simulations are needed.

Our approach is not limited to the case of polystyrene but can be also applied to other polymers. It is especially useful for coarse-grained models in which the mapping scheme is close to the chemical structure and the basic assumption of completely uncorrelated coarse-grained degrees of freedom is not valid. We showed that the previous method can still be used, if the coarse-grained model is constructed in a way that takes into account these correlations and reproduces them also in the coarse-grained simulations. The approach extends the scope and applicability of coarse-grained polymer models as it can easily be extended to multicomponent systems (blends, polymer/solvent mixtures).

Acknowledgment. The authors thank Dirk Reith, Berk Hess, and Victor Rühle for many useful discussions, Giuseppe Milano for providing an initial atomistic configuration of an atactic system of 10-mers, and Valentina Marcon and Christine Peter for carefully reading the manuscript.

Supporting Information Available: Additional figures and notes. This material is available free of charge via the Internet at http://pubs.acs.org.

References and Notes

(1) Tschoep, W.; Kremer, K.; Batoulis, J.; Bürger, T.; Hahn, O. *Acta Polym.* **1998**, *49*, 61–74.
(2) Tschoep, W.; Kremer, K.; Hahn, O.; Batoulis, J.; Bürger, T. *Acta Polym.* **1998**, *49*, 75–79.
(3) Müller-Plathe, F. *ChemPhysChem* **2002**, *3*, 754–769.
(4) Villa, A.; Peter, C.; van der Vegt, N. F. A. *Phys. Chem. Chem. Phys.* **2009**, *11*, 2077–2086.
(5) Villa, A.; van der Vegt, N. F. A.; Peter, C. *Phys. Chem. Chem. Phys.* **2009**, *11*, 2068–2076.
(6) Strauch, T.; Yelash, L.; Paul, W. *Phys. Chem. Chem. Phys.* **2009**, *11*, 1942–1948.
(7) *Coarse-Graining of Condensed Phase and Biomolecular Systems*, 1st ed.; Voth, G. A., Ed.; CRC Press: New York, 2008.
(8) Padding, J.; Briels, W. J. *J. Chem. Phys.* **2002**, *117*, 925–943.
(9) Vettorel, T.; Kremer, K. *J. Chem. Phys.*, submitted.
(10) Murat, M.; Kremer, K. *J. Chem. Phys.* **1998**, *108*, 4340–4348.
(11) Milano, G.; Müller-Plathe, F. *J. Phys. Chem. B* **2005**, *109*, 18609–18619.
(12) Spyriouni, T.; Tzoumanekas, C.; Theodorou, D. N.; Müller-Plathe, F.; Milano, G. *Macromolecules* **2007**, *40*, 3876–3885.
(13) Qian, H.; Carbone, P.; Chen, X.; Varzaneh, H. A. K.; Liew, C. C.; Müller-Plathe, F. *Macromolecules* **2008**, *41*, 9919–9929.
(14) (a) Sun, Q.; Faller, R. *Macromolecules* **2006**, *39*, 812–820. (b) Sun, Q.; Faller, R. *Comput. Chem. Eng.* **2005**, *29*, 2380–2385.
(15) Harmandaris, V. A.; Adhikari, N. P.; van der Vegt, N. F. A.; Kremer, K. *Macromolecules* **2006**, *39*, 6708–6719.
(16) Harmandaris, V. A.; Reith, D.; van der Vegt, N. F. A.; Kremer, K. *Macromol. Chem. Phys.* **2007**, *208*, 2109–2120.
(17) Reith, D.; Pütz, M.; Müller-Plathe, F. *J. Comput. Chem.* **2003**, *24*, 1624–1636.
(18) (a) Mulder, T.; Harmandaris, V. A.; Lyulin, A. V.; van der Vegt, N. F. A.; Kremer, K.; Michels, M. A. J. *Macromolecules* **2009**, *42*, 384–391. (b) Hess, B.; Leon, S.; van der Vegt, N. F. A.; Kremer, K. *Soft Matter* **2006**, *2*, 409–414.
(19) (a) Harmandaris, V. A.; Kremer, K. *Macromolecules* **2009**, *42*, 791–802. (b) Harmandaris, V. A.; Kremer, K. *Soft Matter* **2009**, DOI: 10.1039/b905361a.
(20) Humphrey, W.; Dalke, A.; Schulten, K. *J. Mol. Graphics* **1996**, *14*, 33–38.
(21) Müller-Plathe, F. *Macromolecules* **1996**, *29*, 4782–4791.
(22) Thus, strictly speaking, $V_{\mathrm{PMF}}^{\mathrm{excl,AA}}$ is not a PMF since the sampling was not done with the Hamiltonian for which the forces were evaluated. However, in our tests the difference to a PMF with a repeated sampling was within the error bars. The advantage of reusing the trajectory is a saving of half of the CPU time.
(23) McCoy, J. D.; Curro, J. C. *Macromolecules* **1998**, *31*, 9362–9368.
(24) Fukunaga, H.; Takimoto, J.; Doi, M. *J. Chem. Phys.* **2002**, *116*, 8183–8190.
(25) Are, S.; Katsoulakis, M. A.; Plecháč, P.; Rey-Bellet, L. *Siam J. Sci. Comput.* **2008**, *31*, 987–1015.
(26) Hess, B.; Kutzner, C.; van der Spoel, D.; Lindahl, E. *J. Chem. Theory Comput.* **2008**, *4*, 435–447.
(27) Allen, M. P.; Tildesley, D. J. *Computer Simulation of Liquids*; Clarendon: Oxford, 1987.
(28) Hess, B.; Bekker, H.; Berendsen, H. J. C.; Fraaije, J. G. E. M. *J. Comput. Chem.* **1997**, *18*, 1463–1472.
(29) Berendsen, H. J. C.; Postma, J. P. M.; van Gunsteren, W. F.; DiNola, A.; Haak, J. R. *J. Phys. Chem.* **1984**, *81*, 3684.
(30) Wang, H.; Junghans, C.; Kremer, K. *Eur. Phys. J. E* **2009**, *28*, 221–229.
(31) Auhl, R.; Everaers, R.; Grest, G. S.; Kremer, K.; Plimpton, S. J. *J. Chem. Phys.* **2003**, *119*, 12718–12728.
(32) Boothroyd, A. T.; Rennie, A. R.; Wignall, G. D. *J. Chem. Phys.* **1993**, *99*, 9135–9144.
(33) Fetters, L. J.; Lohse, D. J.; Graessley, W. W. *J. Polym. Sci., Part B: Polym. Phys.* **1999**, *37*, 1023–1033.
(34) Stölken, S.; Ewen, B.; Kobayashi, M.; Nakaoki, T. *J. Polym. Sci., Part B: Polym. Phys.* **1994**, *32*, 881–885.
(35) Reference 34 gives an experimental value of 10.6 for the C_∞ of syndiotactic PS. This value, however, is calculated with a monomer length l_{m} of 2.52 Å. Taking into account carbon−carbon bonds along the backbone (two per monomer) and their bond length l of 1.53 Å gives a value of 14.4 ± 2.8 for the C_∞. This way of defining C_∞ is used in this work as well as in ref 36.
(36) Yoon, D. Y.; Flory, P. J. *Macromolecules* **1976**, *9*, 294–299.
(37) Zoller, P.; Walsh, D. J. *Standard Pressure-Volume-Temperature Data for Polymers*; Technomic: Lancaster, 1995.
(38) Carbone, P.; Varzaneh, H. A. K.; Chen, X.; Müller-Plathe, F. *J. Chem. Phys.* **2008**, *128*, 064904.